Computer Simulation of Convection in Moving Arc Weld Pools

S. KOU and Y. H. WANG

Computer simulation for three-dimensional convection in moving arc weld pools was described, with three distinct driving forces for flow considered — the electromagnetic force, the buoyancy force, and the surface tension gradient on the pool surface. Formulation of the electromagnetic force in the weld pool was presented. The calculated and experimentally observed fusion boundaries were compared. The arc efficiency and spatial distributions of the current density and power density used in the calculations were based on experimentally measured results, in order to verify the model. The effects of the electromagnetic and surface tension forces were discussed.

I. INTRODUCTION

IN a recent report[1] the results of a computer model for convection in arc weld pools were presented, and the effects of weld pool convection on macrosegregation and porosity in the resultant welds were discussed. In the present report the computer simulation of three-dimensional convection in moving arc weld pools is addressed, with emphasis on formulation of the electromagnetic force in the weld pool and mathematical modeling of heat and fluid flow.

Several weld pool convection models have been developed by Oreper *et al.*,[2,3] Chan *et al.*,[4] and Kou *et al.*[5] These models describe two-dimensional convection in stationary weld pools in a semi-infinite workpiece. Since the vast majority of arc welding practices involve a moving heat source and weld pool, and the workpieces are finite in thickness rather than semi-infinite, a 3-D convection model for a moving heat source and a workpiece of finite thickness is expected to be much more useful.

Weld pool convection can strongly affect the structure and properties of the resultant welds. Variations in weld characteristics which are likely to occur from changes in weld pool convection are weld penetration, macrosegregation, gas porosity, solidification structure, undercutting, and surface smoothness. Apparently, the quantitative understanding of convection and heat flow in weld pools is of considerable practical interest. Mathematical models describing convection and heat flow in weld pools are essential, not only because of the quantitative understanding they provide, but also because of the difficulties associated with the experimental measurements of weld pool convection. These difficulties are mainly due to the fact that only surface flow, rather than the overall convection pattern in the weld pool, can be observed. In fact, due to arc glow even the observation of surface flow can be rather inconvenient.

The present work is part of the current study on heat flow and solidification in aluminum welds at the University of Wisconsin-Madison. For this reason, 6061 aluminum alloy is chosen in this work.

II. MATHEMATICAL FORMULATION

Figure 1(a) shows a schematic sketch of an arc welding system; the heat source is moving at a constant speed U.

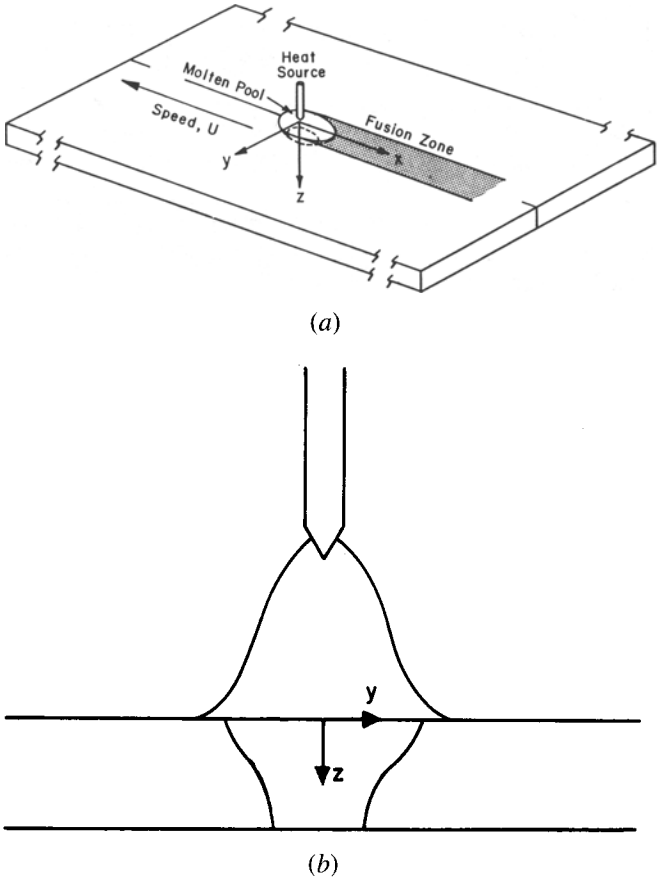

Fig. 1 — Schematic sketch of (*a*) the arc welding system, and (*b*) front view of the arc and the weld pool.

The coordinate system (x, y, z) moves with the heat source at the same speed, and its origin coincides with the center of the electrode. Figure 1(b) is a schematic sketch of the front view of the arc and the weld pool it produces.

There are three distinct driving forces for weld pool convection, *i.e.*, the electromagnetic force, the buoyancy force, and the surface tension gradient at the weld pool surface. The first driving force is caused by the interaction between the divergent current path in the weld pool and the magnetic field it generates. The second driving force is caused by the temperature gradient within the weld pool, and the third by the temperature gradients at the weld pool surface and possibly by the surface active agents in the weld pool.

S. KOU, Professor, and Y. H. WANG, Graduate Student, are with the Department of Metallurgical and Mineral Engineering, University of Wisconsin, Madison, WI 53706.

Manuscript submitted November 11, 1985.

The convection is considered laminar, in view of the small size of the weld pool. The weld pool surface is considered flat, which is reasonable since the GTA (gas tungsten arc) welding process is designed for use with relatively low currents, say around or below 200 A, to avoid melting of the tungsten electrode. It has been reported[6,7] that for a welding current not significantly higher than 200 A, the weld pool surface is flat.

The governing equations for the problem are identical to Eqs. [1] to [3] in the previous paper on convection in laser melted pools,[8] except that the body force, $\mathbf{F}_b$, in the equation of motion should contain not only the buoyancy force but also the electromagnetic force, *i.e.*,

$$\underset{\text{body force}}{\mathbf{F}_b} = \underset{\text{electromagnetic force}}{\mathbf{J} \times \mathbf{B}} - \underset{\text{buoyancy force}}{\rho\beta\mathbf{g}(T - T_0)} \quad [1]$$

The symbols in the above equation are defined at the end of the paper. The third driving force for convection, *i.e.*, the surface tension gradient, is treated as a boundary condition, as will be shown later.

Since the characteristic times associated with electrical conduction are on the order of 10^{-12} second and the welding speed is very low in comparison, the arc can be considered quasi-static. The following set of equations defines the electromagnetic field in the workpiece:

$$\nabla \times \mathbf{E} = 0 \quad [2]$$

$$\nabla \times \mathbf{H} = \mathbf{J} \quad [3]$$

$$\nabla \cdot \mathbf{J} = 0 \quad [4]$$

$$\nabla \cdot \mathbf{B} = 0 \quad [5]$$

where $\mathbf{E}$ and $\mathbf{H}$ are the electric field vector and the magnetic field vector, respectively. The above equations are the steady-state version of Maxwell's equations with the MHD approximation.[9,10,11] The following two equations describe the relationship between $\mathbf{J}$ and $\mathbf{E}$, and $\mathbf{B}$ and $\mathbf{H}$:

$$\mathbf{J} = \sigma_e \mathbf{E} \quad [6]$$

$$\mathbf{B} = \mu_m \mathbf{H} \quad [7]$$

where σ_e and μ_m are the electrical conductivity and magnetic permeability, respectively. Equation [6] is a good approximation when the secondary current induced by the convective motion of the liquid metal is not very high.[9] The current distribution on the weld pool surface, *i.e.*, $z = 0$, can be described by the following function:[2]

$$J_z = \frac{3I}{\pi b^2} \exp\left(\frac{-3r^2}{b^2}\right) \qquad \text{at } z = 0 \quad [8]$$

where J_z is the z-component of $\mathbf{J}$, I the welding current, b the effective radius of the current distribution, and r the radius, *i.e.*, $(x^2 + y^2)^{1/2}$.

While the boundary condition for current flow is described by Eq. [8] at the top surface of the workpiece, the corresponding boundary condition at the bottom surface is as follows:

$$J_z = 0 \qquad \text{at } z = g \quad [9]$$

where g is the thickness of the workpiece. In other words, the bottom surface of the workpiece is electrically insulated, *e.g.*, by a ceramic backing or just an air gap.

It should be pointed out that in practical welding, the size of the weld pool is far smaller than that of the workpiece. As such, the ground effect, which is undesirable and can be easily avoided in most cases anyway, is negligible. In fact, even in small laboratory-scale welding experiment (*e.g.*, 20.3 cm × 12.7 cm × 3.2 mm aluminum plates in the present study), the ground effect is negligible. This is because the ground cable is seldom connected directly to the workpiece or fixture, but to the welding table. In the experiments of Lawson *et al.*,[12] where the ground effect was studied, small coupons were welded, with the ground connection purposely located on the coupons and with the welding table electrically isolated from the coupons.

From Eqs. [2] to [9], the electromagnetic force $\mathbf{J} \times \mathbf{B}$ can be expressed as follows:

$$\mathbf{J} \times \mathbf{B} = B_\theta(J_r\mathbf{z} - J_z\mathbf{r}) \quad [10]$$

where

$$J_z = \frac{1}{2\pi}\int_0^\infty \lambda J_0(\lambda r)\exp(-\lambda^2 b^2/12)\frac{\sinh \lambda(g - z)}{\sinh \lambda g}\, d\lambda \quad [11]$$

$$J_r = \frac{I}{2\pi}\int_0^\infty \lambda J_1(\lambda r)\exp(-\lambda^2 b^2/12)\frac{\cosh \lambda(g - z)}{\sinh \lambda g}\, d\lambda \quad [12]$$

$$B_\theta = \frac{\mu_m I}{2\pi}\int_0^\infty J_1(\lambda r)\exp(-\lambda^2 b^2/12)\frac{\sinh \lambda(g - z)}{\sinh \lambda g}\, d\lambda \quad [13]$$

J_r is the r-component of $\mathbf{J}$ and B_θ is the θ-component of $\mathbf{B}$, where θ is the third independent variable in the cylindrical coordinate system (r, z, θ). J_0 and J_1 are the Bessel functions of the first kind and of the zero and first order, respectively.

The boundary conditions are similar to those described previously for convection in laser melted pools[8] and hence will not be repeated here. On the top surface of the workpiece, the heat flux q can be expressed as follows:

$$q = \begin{cases} \dfrac{3\eta EI}{\pi a^2}\exp\left(\dfrac{-3r^2}{a^2}\right) & \text{for } r \le a \\ h(T - T_a) + \sigma e(T^4 - T_a^4) & \text{for } r > a \end{cases} \quad [14]$$

The first equation describes the heat input due to the arc, while the second the heat loss due to convection and radiation, which is very small in the welding of aluminum due to its low melting temperature and high conductivity.

III. METHOD OF SOLUTION

The method of solution described in a previous report on convection in stationary weld pools[5] was adopted in the present study. In short, the governing equations with the boundary conditions were solved using the finite difference method. As described previously, the enthalpy-temperature and viscosity-temperature relationships for both the solid and liquid phases were used, thus allowing the heat of solidification and the zero velocity at the pool boundary to be

incorporated automatically in the heat and fluid flow calculation. As a result, the tedious work of tracking the pool boundary during each iteration of computation is not required and the computation time was reduced significantly.

As in the previous report, the SIMPLE (Semi-Implicit Method for Pressure-Linked Equations) algorithm was employed for the calculation of velocity field. A detailed description of this algorithm is available elsewhere.[13,14,15]

Due to symmetry with respect to the center plane (*i.e.*, the *x-z* plane), the velocity and temperature fields were calculated on only one side of the center plane. In order to enhance the accuracy of calculation, grids of variable spacing were used, *i.e.*, finer spacing near the heat source and coarser away from it. For calculations where steep velocity gradients $\partial u/\partial z$ and $\partial v/\partial z$ are induced by the surface tension gradient at the pool surface, the use of the fine grid spacing near the surface is essential.

The grid system used consisted of four different grids: three for the *x*-, *y*-, and *z*-components of the velocity and body force, and one for the scalars. Such a grid system, called the "staggered grid", is required for numerical stability in fluid flow calculations.[13,16,17]

A UNIVAC computer was employed to carry out the computation. The iterative procedure was continued until the following convergence criterion was satisfied:

$$\frac{\Sigma_p |\phi - \phi^{\text{old}}|}{\Sigma_p |\phi|} < 0.001$$

where Σ_p denotes summation over all grid points, and ϕ is the variable being computed, *e.g.*, *u*, *v*, or *w*. The physical properties used are shown in Table I.

IV. RESULTS AND DISCUSSION

Figure 2 shows the comparison between the calculated and observed fusion boundaries for a GTA weld made in a 3.2 mm thick 6061 aluminum plate. The current, voltage, and speed of welding were 110 A, 10 V, and 5.5 mm/sec, respectively. A tungsten-2 pct thoria electrode of 2.4 mm diameter and 50 deg tip angle was used. The shielding gas was pure argon. The arc efficiency η, the heat flux radius, and the current flux radius used in the calculation are 76 pct, 3.0 mm, and 2.0 mm, respectively. The arc efficiency was measured calorimetrically using a 38 mm × 38 mm square tube of the workpiece material. The tube was insulated from the surroundings, and the difference between the inlet and outlet water temperatures was measured using differential thermistors. From the temperature difference, the water flow rate and the welding time, the arc efficiency can be determined, as described elsewhere.[21] The spatial distributions of the heat flux and current flux were measured using

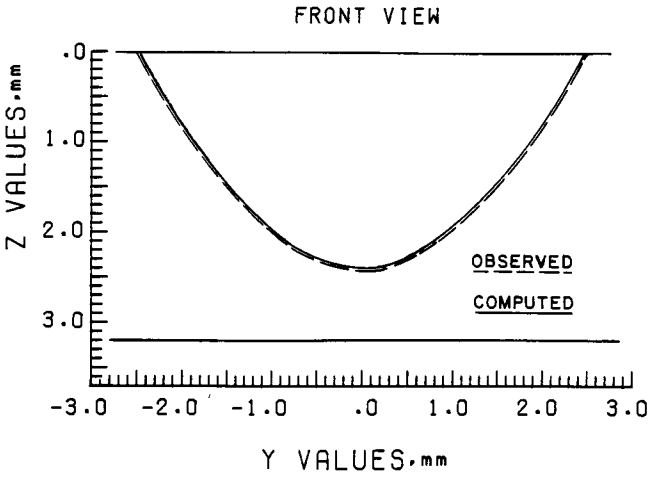

Fig. 2—Comparison between calculated and observed fusion boundaries.

the "split anode method". Details of the experimental procedure and treatment of data will be presented elsewhere.[22] As shown in Figure 2, the agreement between the calculated and observed fusion boundaries is very good.

Figure 3 shows the computed isotherms and convection patterns in the pool of the weld shown previously in Figure 2. As can be seen from the top and side views, the weld is not symmetrical with respect to the center of the electrode, *i.e.*, the origin. The front of the weld pool surface is about 2 mm ahead of the origin, while the tail is 3 mm behind. In other words, the problem is no longer two dimensional but three dimensional, due to the travel of the heat source. Of course, if the travel speed of the heat source were much higher, the deviations in the pool shape and convective flow patterns from symmetry would have been much more pronounced. However, this would also have prevented the computer model from being verified. This is because at high welding speeds, the arc is no longer symmetrical and the split-anode data are useless. Also, thermal undercooling in the weld pool becomes significant and the weld pool boundary can no longer be defined by the liquidus isotherm.

As can be seen in the front view of the convection pattern in Figure 3(a), there are two circulation loops in the weld pool—one near the free surface and the other in the bulk weld pool. The maximum velocity, which occurs at the free surface, is 2.3×10^3 mm/sec. Surface velocities on the order of 10^3 mm/sec have been observed recently by Heiple *et al.*[23] Figure 3(b) shows the top view of the convection pattern. As shown, flow at the free surface is radially outward, from the axis of the electrode (*z*-axis) to the pool boundary. Figure 3(c) shows the side view of the convection pattern. As shown, there are two circulation loops both ahead and behind the electrode, being consistent with the

Table I. Physical Properties Used for Calculation[18,19,20]

$\beta = 1.0 \times 10^{-4}$ °C^{-1}	$\rho = 2700$ Kg/m^3
$\mu_m = 1.26 \times 10^{-6}$ Henery/m	$C_S = 1066$ Joules/Kg °C
$\partial\gamma/\partial T = -0.35 \times 10^{-3}$ Kg/sec^2 °C	$C_L = 1066$ Joules/Kg °C
$T_L = 652$ °C	$k_S = 168$ Watt/m °C
$T_S = 582$ °C	$k_L = 108$ Watt/m °C
$T_a = 25$ °C	$\mu_S = 1.0 \times 10^5$ Kg/m sec
$\Delta H = 3.95 \times 10^5$ Joules/Kg	$\mu_L = 1.0 \times 10^{-3}$ Kg/m sec

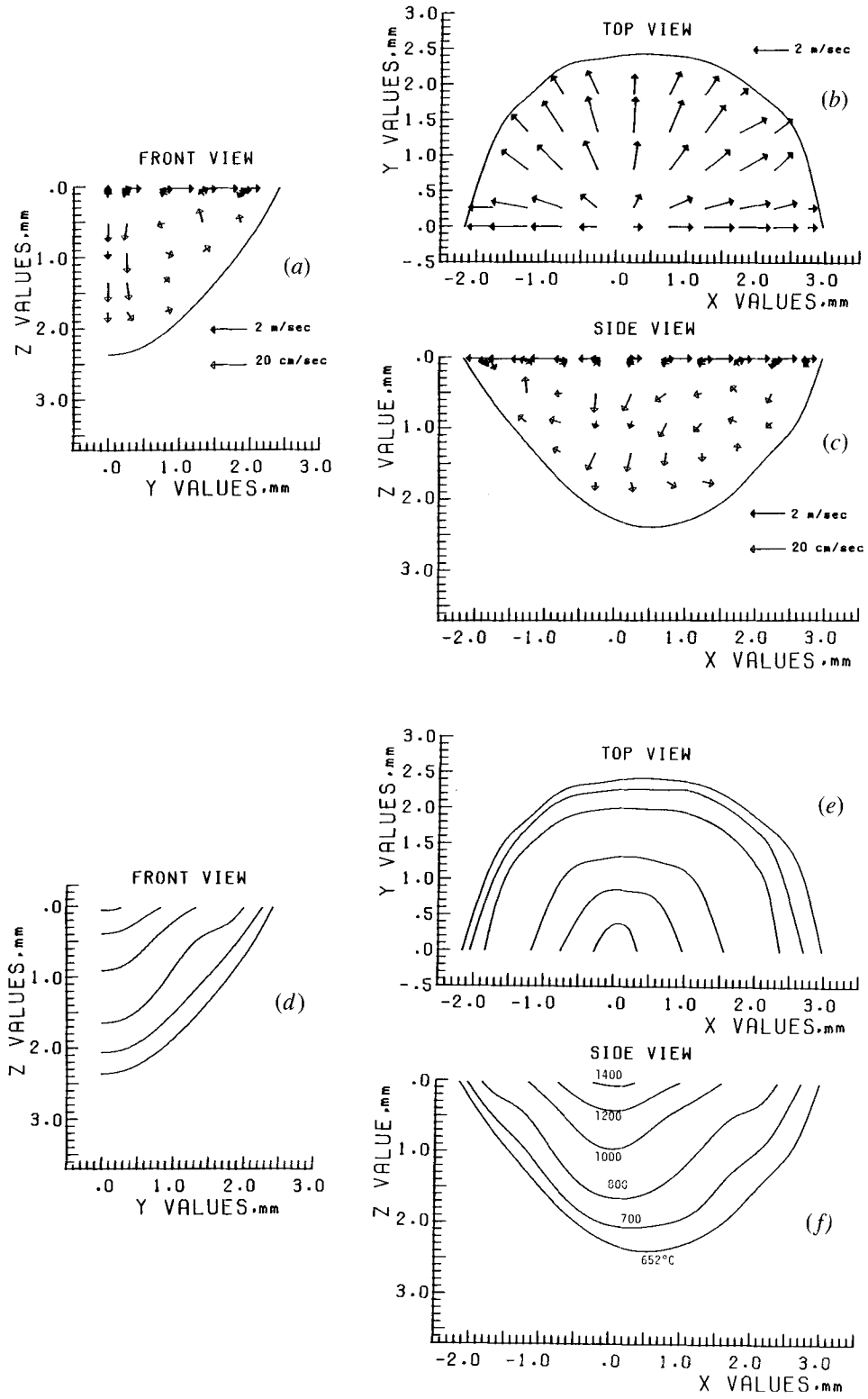

Fig. 3—Calculated velocity and temperature fields in the weld pool.

results shown previously in Figure 3(a). The corresponding isotherms are shown in Figures 3(d) to 3(f).

The first circulation loop near the pool surface mentioned above is due to the surface tension gradient at the pool surface, *i.e.*, the so-called "Marangoni flow". The surface tension temperature coefficient is negative, *i.e.*, $\partial\gamma/\partial T = -0.35 \times 10^{-3}$ Kg/sec^2 °C. Consequently, the surface tension is lower near the center of the weld pool surface, where the temperature is higher, and is higher near the pool boundary, where the temperature is lower. There-

fore, the liquid metal near the center of the weld pool surface is driven toward the pool boundary, resulting in a radially outward flow pattern on the pool surface.

The second circulation loop in the bulk weld pool is due to the electromagnetic force. Due to the interaction between the divergent current path in the weld pool and the magnetic field it generates, a downward pushing action is produced along the z-axis, resulting in downward flow of the liquid metal in that region.

Figure 4 shows the effect of the electromagnetic force on weld pool convection and weld penetration. Figure 4(a) shows the convection pattern produced by the electromagnetic force alone, the input parameters being the same as those used previously in Figure 3, except that the buoyancy and surface tension forces are excluded. As shown in Figure 4(b), when the current flux radius is increased from 2 mm to 3 mm, the weld switches from full to partial penetration, even though the energy input remains the same. This is because the larger the current flux radius, the less divergent the current path and the smaller the electromagnetic force become in the weld pool. This is reflected by the change in the calculated maximum velocity in the weld pool; *i.e.*, the maximum velocity decreases with increasing current flux radius.

Figure 5 shows the effect of the surface tension temperature coefficient $\partial\gamma/\partial T$ on weld pool convection and weld penetration. Figure 5(a) shows the convection pattern produced by the surface tension force alone, the input parameters being the same as those used previously in Figure 3, except that the buoyancy and electromagnetic forces are excluded. As shown in Figure 5(b), when the value of the surface tension temperature coefficient is changed from -0.35×10^{-3} Kg/sec^2 °C to $+0.35 \times 10^{-3}$ Kg/sec^2 °C, the convection pattern is reversed and the weld switches from partial to full penetration, even though the energy input remains the same. This is because when the surface tension temperature coefficient becomes positive, the liquid metal flows toward the center of the pool surface where it picks up the arc energy and delivers it down to the weld root, thus producing a deeper penetration.

The effect of the surface tension temperature coefficient described above is consistent with the recent experimental work of Heiple.[24] In short, it was shown that, with a very small addition of SO_2(g) in the argon shielding gas, GTA welds in 304L stainless steel changed from partial to full penetration. Both sulfur and oxygen, which are produced by the decomposition of SO_2(g) in the arc, are surface active agents for liquid iron and tend to reduce or even reverse its surface tension *vs* temperature relationship.[25,26,27] Although similar surface active agents are not known in aluminum alloys, the effect of $\partial\gamma/\partial T$ demonstrated in this study is equally applicable to all materials.

It should be pointed out that in the previous experimental work of Heiple *et al.*,[23] shallower penetration was observed in weld pools exhibiting a radially outward surface flow pattern, while deeper penetration was observed in weld pools exhibiting a radially inward surface flow pattern. This is also consistent with the calculated results shown in Figure 5.

V. CONCLUSIONS

1. Three-dimensional convection in moving arc weld pools can be simulated with the computer model developed. The model incorporates three distinct driving forces for flow, *i.e.*, the electromagnetic force, the buoyancy force, and the surface tension gradient on the pool surface.

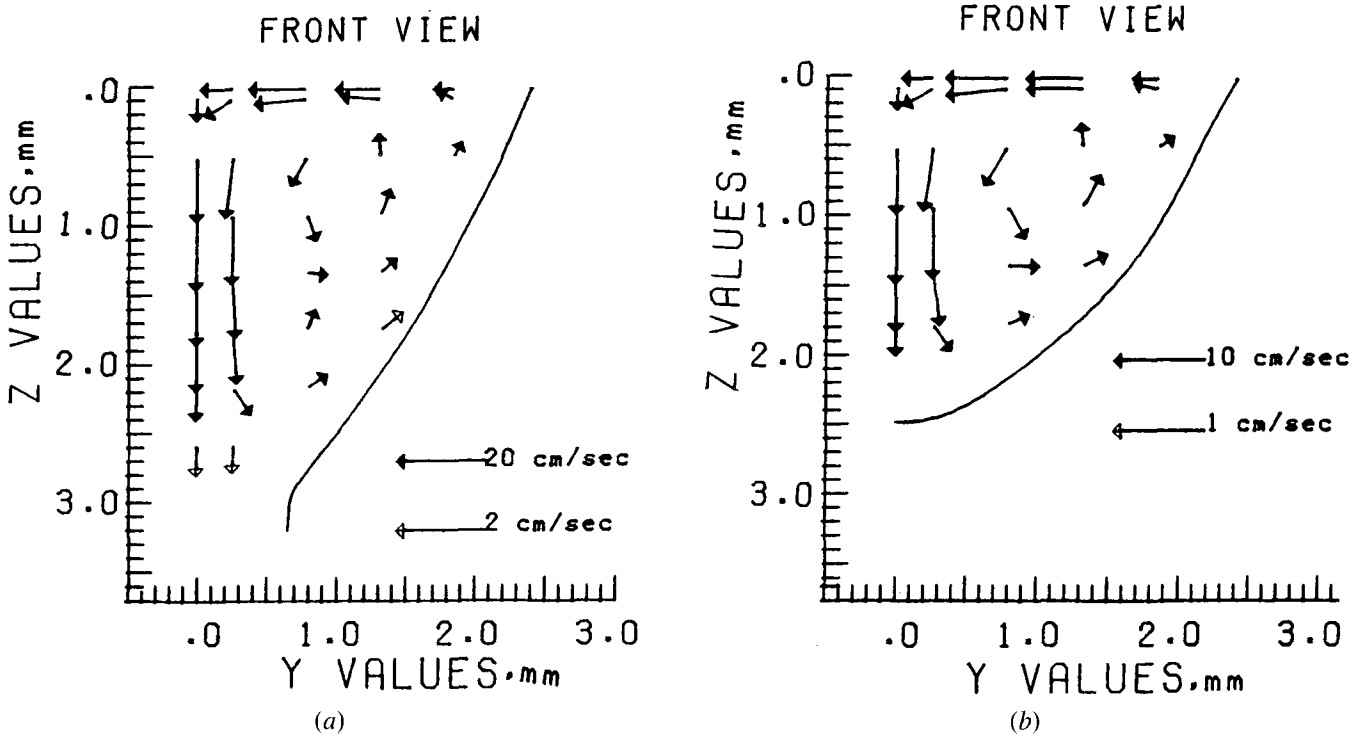

Fig. 4—Effect of the electromagnetic force on convection pattern and weld penetration: (*a*) current flux radius = 2 mm; (*b*) current flux radius = 3 mm.

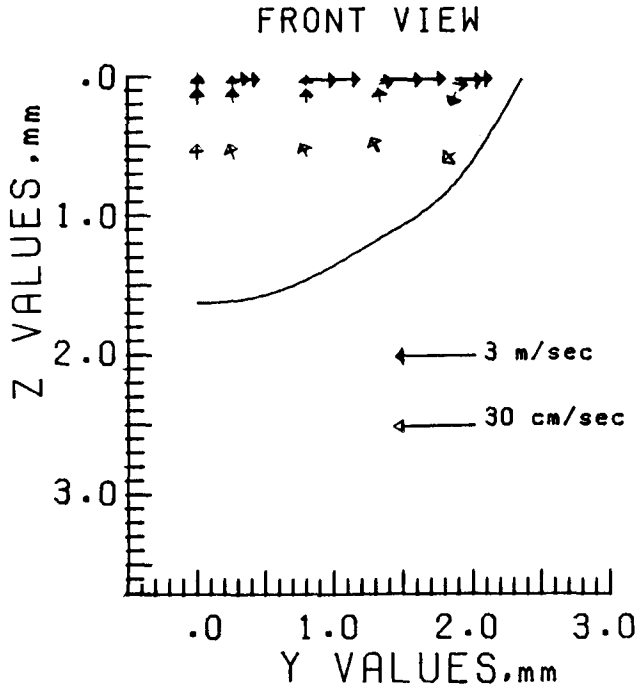

(*a*)

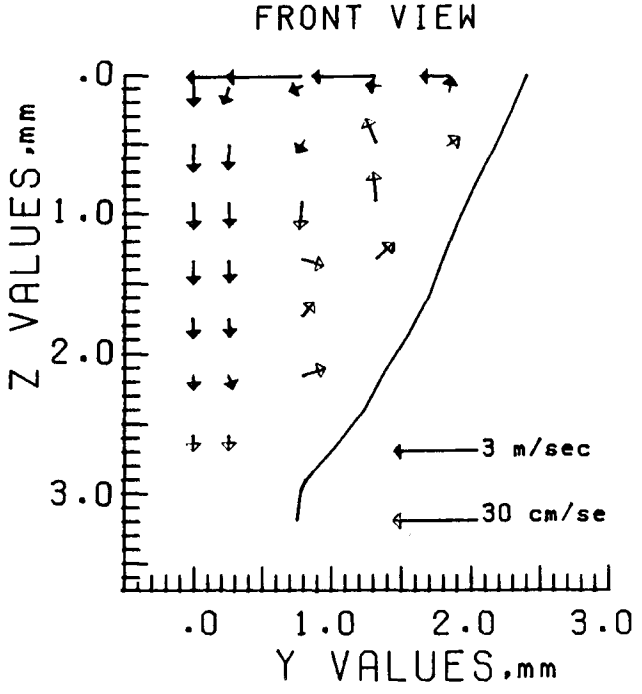

(*b*)

Fig. 5—Effect of the surface tension temperature coefficient on convection pattern and weld penetration: (*a*) $\partial\gamma/\partial T = -0.35\times10^{-3}$ Kg/sec^2 °C; (*b*) $\partial\gamma/\partial T = 0.35\times10^{-3}$ Kg/sec^2 °C.

Formulation for the electromagnetic force in the weld pool has been presented.

2. Based on the measured arc efficiency and the spatial distributions of the current density and power density in the arc, the calculated and observed fusion boundaries were compared and very good agreement was obtained.
3. The model demonstrates the effect of the electromagnetic force on weld pool convection and the penetration of the resultant weld.
4. The effect of the surface tension temperature coefficient demonstrated with the computer model is consistent with the experimental observations of Heiple *et al.*

SYMBOLS AND DEFINITIONS

a	heat flux radius
b	current flux radius
$\mathbf{B}$	magnetic flux vector
C_L	specific heat of liquid
C_S	specific heat of solid
e	total emissivity
E	welding voltage
$\mathbf{E}$	electric field vector
$\mathbf{F}_b$	body force
g	workpiece thickness
$\mathbf{g}$	gravitational acceleration
h	heat transfer coefficient
$\mathbf{H}$	magnetic field vector
ΔH	heat of fusion
I	welding current
J_r	radial component of current density vector
J_z	axial component of current density vector
$\mathbf{J}$	current density vector
k	thermal conductivity
k_L	thermal conductivity of liquid
k_S	thermal conductivity of solid
q	heat flux
T	temperature
T_a	ambient temperature
T_0	reference temperature
T_L	liquidus temperature
T_S	solidus temperature
U	welding speed
u	x-component of velocity vector
v	y-component of velocity vector
w	z-component of velocity vector
x, y, z	coordinates
β	thermal expansion coefficient
γ	surface tension
$\partial\gamma/\partial T$	surface tension temperature coefficient
η	arc efficiency
μ	viscosity
μ_L	viscosity of liquid
μ_m	magnetic permeability
μ_S	viscosity of solid
ρ	density
σ	Stefan-Boltzmann constant

ACKNOWLEDGMENT

The authors gratefully acknowledge support for this study from the National Science Foundation, under NSF Grant No. DMR 8419274.

REFERENCES

1. S. Kou and Y. H. Wang: *Weld. J.*, 1986, vol. 65, p. 63s.
2. G. M. Oreper, T. W. Eagar, and J. Szekely: *Weld. J.*, 1983, vol. 62, p. 307s.
3. G. M. Oreper and J. Szekely: *J. Fluid Mechanics*, 1984, vol. 147, p. 53.
4. C. Chan, J. Mazumder, and M. M. Chen: *Metall. Trans. A*, 1984, vol. 15A, p. 2175.
5. S. Kou and D. K. Sun: *Metall. Trans. A*, 1985, vol. 16A, p. 203.
6. W. H. S. Lawson and H. W. Kerr: *Welding Research International*, 1976, vol. 6, p. 1.
7. M. L. Lin and T. W. Eagar: *Weld. J.*, 1985, vol. 64, p. 163s.
8. S. Kou and Y. H. Wang: *Metall. Trans. A*, 1986, vol. 17A, p. 2265.
9. S. Szekely: *Fluid Flow Phenomena in Metals Processing*, Academic Press, New York, NY, 1979, p. 178.
10. W. F. Hughes and F. J. Young: *The Electromagnetodynamics of Fluids*, John Wiley, New York, NY, 1966, ch. 7.
11. J. D. Jackson: *Classical Electrodynamics*, 2nd ed., John Wiley, New York, NY, 1976, ch. 3.
12. W. H. S. Lawson and H. W. Kerr: *Welding Research International*, 1976, vol. 6, p. 63.
13. S. V. Patankar and D. B. Spalding: *Int. J. Heat and Mass Transfer*, 1972, vol. 15, p. 1787.
14. S. V. Patankar and D. B. Spalding: *Proc. 14th Symp. on Combustion*, The Combustion Inst., 1972, p. 605.
15. L. S. Caretto, A. D. Gosman, S. V. Patankar, and D. B. Spalding: *Proc. 3rd Int. Conf. Num. Methods Fluid Dyn.*, Paris, 1972, vol. II, p. 60.
16. F. H. Harlow and J. E. Welch: *Phys. Fluids*, 1965, vol. 8, p. 2182.
17. L. S. Caretto, R. M. Curr, and D. B. Spalding: *Comp. Methods Appl. Mech. Eng.*, 1972, vol. 1, p. 39.
18. B. C. Allen: in *Liquid Metals–Chemistry and Physics*, S. Z. Beer, ed., M. Dekker, Inc., New York, NY, 1972, p. 161.
19. *Aluminum Standards and Data*, 5th ed., The Aluminum Association, New York, NY, 1976, p. 38 and p. 40.
20. *Aluminum*, K. R. Van Horn, ed., ASM, 1967, vol. 1, ch. 1, pp. 1-30.
21. S. Kou and Y. Le: *Metall. Trans. A*, 1984, vol. 15A, p. 1165.
22. M. Lu and S. Kou: unpublished work at University of Wisconsin, Madison, WI, 1985.
23. C. R. Heiple and J. R. Roper: *Weld. J.*, 1982, vol. 61, p. 97s.
24. C. R. Heiple and P. Burgardt: *Weld. J.*, 1985, vol. 64, p. 159s.
25. T. T. Van, R. A. Karasev, and A. M. Samarin: *Russian Metallurgy and Fuels*, 1960, vol. 2, p. 33.
26. K. M. Gupt, V. I. Yavoiski, A. F. Vishkaryov, and S. A. Bliznukov: *Trans. Indian Inst. Metals*, 1976, vol. 29, p. 286.
27. S. I. Popel, B. V. Tsarevskiy, V. V. Pavlov, and E. L. Furman: *Russian Metallurgy*, 1975, (4), p. 42.